



Morard, G., Nakajima, Y., Andrault, D., Antonangeli, D., Auzende, A. L., Boulard, E., ... Mezouar, M. (2017). Structure and density of Fe-C liquid alloys under high pressure. *Journal of Geophysical Research: Solid Earth*, 122(10), 7813-7823. <https://doi.org/10.1002/2017JB014779>

Publisher's PDF, also known as Version of record

Link to published version (if available):

[10.1002/2017JB014779](https://doi.org/10.1002/2017JB014779)

[Link to publication record in Explore Bristol Research](#)

PDF-document

This is the final published version of the article (version of record). It first appeared online via AGU publications at <http://onlinelibrary.wiley.com/doi/10.1002/2017JB014779/abstract>. Please refer to any applicable terms of use of the publisher.

University of Bristol - Explore Bristol Research

General rights

This document is made available in accordance with publisher policies. Please cite only the published version using the reference above. Full terms of use are available: <http://www.bristol.ac.uk/pure/about/ebr-terms>

RESEARCH ARTICLE

10.1002/2017JB014779

Key Points:

- Structure and density of liquid Fe-C alloys were measured up to 58 GPa and 3,200 K
- An 8–16 at % C (1.8–3.7 wt % C) could to explain the density deficit of the outer core
- Carbon cannot be the only light element alloyed to iron in the Earth's core

Correspondence to:

G. Morard,
guillaume.morard@imPMC.upmc.fr

Citation:




Morard, G., Nakajima, Y., Andrault, D., Antonangeli, D., Auzende, A. L., Boulard, E., ... Mezouar, M. (2017). Structure and density of Fe-C liquid alloys under high pressure. *Journal of Geophysical Research: Solid Earth*, 122. <https://doi.org/10.1002/2017JB014779>

Received 28 JUL 2017

Accepted 15 OCT 2017

Accepted article online 19 OCT 2017

Structure and Density of Fe-C Liquid Alloys Under High Pressure

G. Morard¹ , Y. Nakajima^{2,3} , D. Andrault⁴, D. Antonangeli¹, A. L. Auzende^{1,5}, E. Boulard⁶, S. Cervera¹, A. N. Clark¹, O. T. Lord⁷, J. Siebert⁸, V. Svitlyk⁹ , G. Garbarino⁹, and M. Mezouar⁹

¹Institut de Minéralogie, de Physique des Matériaux, et de Cosmochimie (IMPMC), Sorbonne Universités - UPMC, UMR CNRS 7590, Muséum National d'Histoire Naturelle, Paris, France, ²Materials Dynamics Laboratory, RIKEN SPring-8 Center, RIKEN, Hyogo, Japan, ³Department of Physics, Kumamoto University, Kumamoto, Japan, ⁴Laboratoire Magmas et Volcans, CNRS-OPGC-IRD, Université Blaise Pascal, Clermont-Ferrand, France, ⁵ISTerre, Université Grenoble Alpes, CNRS, Grenoble, France, ⁶Synchrotron Soleil, L'Orme des Merisiers, Saint Aubin, France, ⁷School of Earth Sciences, University of Bristol, Bristol, UK, ⁸Institut de Physique du Globe de Paris, Paris, France, ⁹European Synchrotron Radiation Facility, Grenoble, France

Abstract The density and structure of liquid Fe-C alloys have been measured up to 58 GPa and 3,200 K by in situ X-ray diffraction using a Paris-Edinburgh press and laser-heated diamond anvil cell. Study of the pressure evolution of the local structure inferred by X-ray diffraction measurements is important to understand the compression mechanism of the liquid. Obtained data show that the degree of compression is greater for the first coordination sphere than the second and third coordination spheres. The extrapolation of the measured density suggests that carbon cannot be the only light element alloyed to iron in the Earth's core, as 8–16 at % C (1.8–3.7 wt % C) would be necessary to explain the density deficit of the outer core relative to pure Fe. This concentration is too high to account for outer core velocity. The presence of other light elements (e.g., O, Si, S, and H) is thus required.

1. Introduction

Geological and cosmochemical observations show that, in addition to iron, lighter elements such as hydrogen, carbon, oxygen, silicon, and sulfur are expected to be present in the Earth's core (McDonough, 2003; Poirier, 1994) and more generally in the metallic core of terrestrial planets throughout the solar system. These lighter elements modify the chemical activity, the physical properties, and the phase diagram of iron. The light elements are known to have a strong influence on the distributions of other elements between core forming metals and silicate magma oceans during core formation processes (Fischer et al., 2015; Siebert et al., 2013), to affect the thermal conductivity of the core (de Koker et al., 2012) and the melting temperature of the core alloy (Morard, Andrault, et al., 2014). Constraining the identity and concentration of these light elements is, in turn, key to understanding the dynamics of the core including its formation processes, thermal evolution, and the present-day core geotherm. The primary information available for the Earth's core are density and velocity profiles provided by seismological observations, so it is critically important to experimentally determine the elastic properties of iron alloys under *P-T* conditions of planetary cores.

Carbon is often cited as a potential light element alloyed with iron in the Earth's core because of its chemical affinity with the metallic phase and high cosmochemical abundance. Indeed, it is commonly found in carbonate chondrites and iron meteorites. Carbon easily dissolves in liquid Fe over a wide pressure range from ambient to high pressures (Lord et al., 2009; Nakajima et al., 2009), and it strongly partitions into the liquid metallic phase, compared to silicate melts, at *P-T* conditions relevant to core formation (Chi et al., 2014; Dasgupta & Walker, 2008). Recent experimental measurements and theoretical calculations on the elastic properties of Fe₇C₃ put ahead the idea that a C-rich solid inner core could reasonably explain the seismological observations of density, sound velocity, and Poisson's ratio (Chen et al., 2014; Mookherjee, 2011; Nakajima et al., 2011; Prescher et al., 2015). Based on the Fe-C phase diagram at high pressure, the Fe₇C₃ phase could solidify at the inner-outer core boundary if the liquid core contains more than 2 wt % carbon (Fei & Brosh, 2014; Liu et al., 2016). A model where Fe₇C₃ is a candidate component of the inner core requires a careful evaluation in light of the total carbon content of the Earth's core.

In the present study, we report new experimental data on the structure and density of liquid Fe-C at extreme conditions, increasing the pressure range of density measurements by 1 order of magnitude. In addition, the

pressure-induced variation of the local structure of the liquid alloy is studied and the compression mechanism is described.

2. Materials and Methods

2.1. High-Pressure Experiments

Experiments to collect diffuse X-ray scattering of liquid Fe-C alloys were performed in situ at high pressures and temperatures by angle dispersive X-ray diffraction measurements in the Paris-Edinburgh press (PEP) below 10 GPa and the double-sided laser-heated diamond anvil cell (LH-DAC) above 40 GPa (Beamline ID27 of the European Synchrotron Radiation Facility (ESRF) in Grenoble, France (Mezouar et al., 2005)). For the LH-DAC experiments, starting materials with initial composition of Fe + 1.5 wt % C (6.6 at % C) were synthesized by an ultrarapid quench method at the Institut de Chimie et des Matériaux de Paris-Est (ICMPE), Paris, France (Morard et al., 2017), whereas for the PEP experiments the starting material was composed of a mixture of pure Fe (Alfa Aesar, 99.9%) and graphite powders.

2.1.1. Paris-Edinburgh Press Experiments

Large-volume experiments were carried out using a VX5 type PEP (Besson et al., 1992; Klotz et al., 2005). This press has a large opening angle along the equatorial plane. The very high brilliance X-ray beam delivered by two in vacuum undulators was collimated down to a cross section of $50 \times 50 \mu\text{m}$ (typical values). The X-ray wavelength was fixed to $\lambda = 0.24678 \text{ \AA}$ (Gadolinium K-edge) using a Si(111) channel cut monochromator. A multichannel collimator (Mezouar et al., 2002; Morard, Mezouar, et al., 2011) was used to suppress the X-ray background coming from the sample environment. The diffracted X-rays were collected using a MAR345 imaging plate system (marXperts GmbH, Norderstedt, Germany). The sample detector distance was calibrated with a LaB_6 standard, and the diffraction images were treated and integrated using the Fit2D software (Hammersley et al., 1996).

The high-pressure chamber consisted of two opposed tungsten carbide anvils that have quasi-conical hollows. We used 7 mm boron epoxy gaskets with a classical cell assembly consisting of a graphite cylinder furnace and an MgO capsule acting as both pressure medium and electrical insulator (Mezouar et al., 1999). Pressure was calibrated using the equation of state (EoS) of MgO (Utsumi et al., 1998). The temperature was determined from the measured electrical power using a previously established calibration curve (Morard, Mezouar, et al., 2007). As discussed in a previous paper (Morard, Sanloup, et al., 2007), metrological uncertainties are the following: 170 K in temperature and 0.6 GPa in pressure.

2.1.2. Laser-Heated Diamond Anvil Cell Experiments

LH-DAC experiments were carried out with Le Toullec-type diamond anvil cells equipped with $250 \mu\text{m}$ diameter flat culets diamonds. Diamonds with conical supports (Boehler & De Hantsetters, 2004) were used in order to collect X-ray diffraction over a wide 2θ angle (70°). Flakes of the Fe + 1.5 wt % C with a thickness of $\sim 10 \mu\text{m}$ and a diameter of $\sim 50 \mu\text{m}$ were loaded between two dry KCl layers in $120 \mu\text{m}$ diameter holes drilled in preindented rhenium gaskets. KCl acts as a soft pressure medium at high temperature, ensuring good hydrostatic conditions, with the further advantage of being chemically inert with respect to the iron alloy sample (no reaction has been observed from the analysis of the diffraction patterns of quenched samples). The KCl medium also provides a leak-proof container for liquid metal, which enables the collection of a strong diffuse scattering signal.

Samples were heated on both sides by two continuous fiber YAG lasers (TEM 00) providing a maximum total power of 200 W. Temperatures were obtained by the spectroradiometric method, using reflective collecting optics (Schultz et al., 2005). Laser spots were more than $20 \mu\text{m}$ in diameter. Temperature was measured at the center of the hot spot by analyzing the pyrometric signal emitted by a $2 \times 2 \mu\text{m}^2$ area. The input power of the two lasers was tuned so as to obtain temperature on both sample sides within less than 100 K differences.

Typical exposure times for diffuse scattering measurements were between 5 and 10 s. Temperature uncertainties are essentially related to radial and axial temperature gradients. Considering the $>20 \mu\text{m}$ diameter laser spot and the $4 \mu\text{m}$ diameter X-ray beam used in this study, the uncertainty in the radial direction is less than 50 K (Schultz et al., 2005). The double-sided laser heating and the controlled geometry of the assembly maintain the uncertainty in the axial direction below 100 K. We therefore assume a temperature uncertainty of $\pm 150 \text{ K}$ for our experiments (Morard, Andrault, et al., 2011).

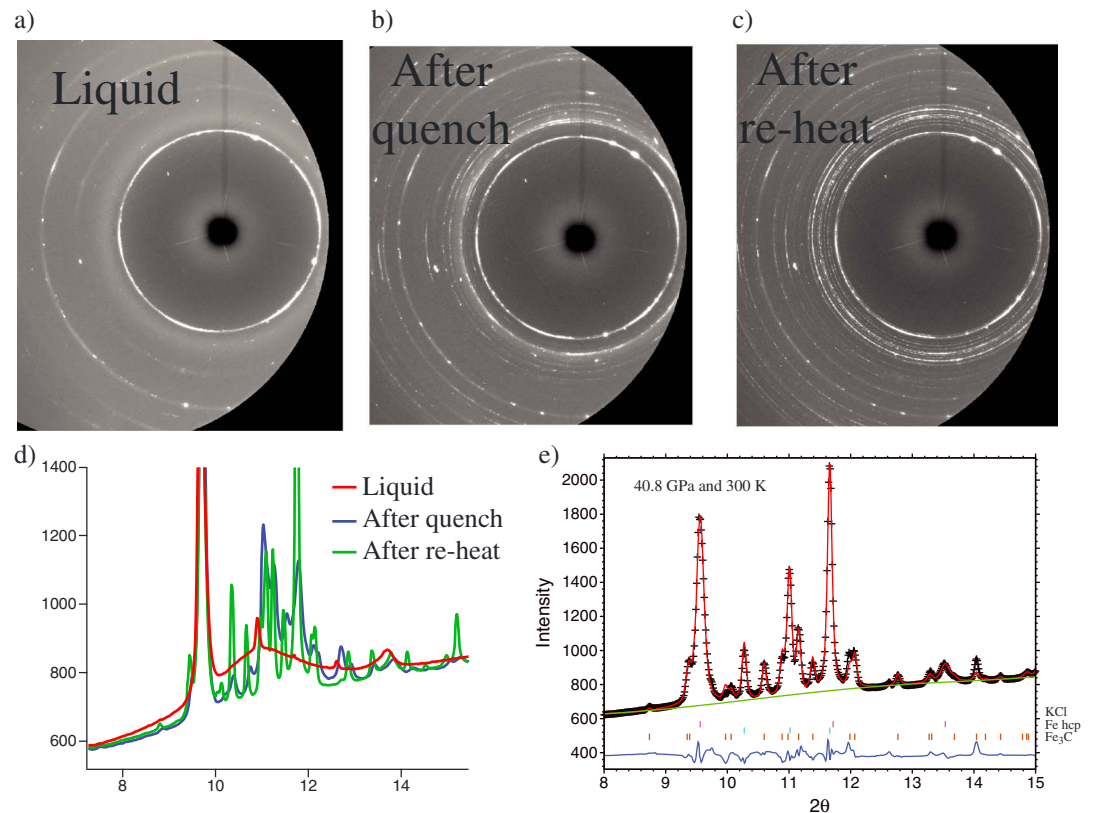


Figure 1. Three diffraction patterns recorded (a) at high temperature in the liquid state (the main diffraction rings still present are from the KCl pressure medium), (b) after quenching by cutting the power to the lasers, and (c) after reheating the sample at 1,380 K (Table 1), well below the melting point of $\sim 2,200$ K at 41 GPa (Liu et al., 2016; Morard et al., 2017). (d) Integrated diffraction patterns from the diffraction patterns shown above and (e) Rietveld analysis of the reheated diffraction pattern. This analysis is used to define the liquid composition, with the assumption of no carbon solubility in solid Fe.

Pressure was determined using the thermal equation of state of KCl (Dewaele et al., 2012). Following Campbell et al. (2009), the temperature of the KCl is assumed to be the average between the temperature of the diamond culet at 300 K and the temperature measured at the sample surface (in view of the high thermal conductivity of diamond, the entire anvil is assumed to be at room temperature). Pressure uncertainties are estimated from the width of the KCl diffraction peaks (± 1 GPa) and the uncertainty in the temperature measurement. The present method has been already used in our previous publication regarding the eutectic melting curve in the Fe-Fe₃C system (Morard et al., 2017).

2.2. Determination of the Chemical Composition of the Liquid Alloys

After quenching the liquid by turning off the laser, the diffuse signal was still observed, suggesting that the quenched alloy exhibited a quasi-amorphous pattern. This amorphous (or very finely grained) sample was then reheated around $\sim 1,400$ K for several minutes in order to obtain well-defined diffraction rings (Figure 1). These high-quality powder diffraction patterns show negligible preferential orientation and allowed us to perform a Rietveld analysis, in order to extract the relative proportions of the resulting assemblage Fe + Fe₃C.

Solubility of carbon in solid Fe has been estimated to be lower than 1 wt % C for pressures higher than 40 GPa (Lord et al., 2009). Yet we observe a volume increase of $\sim 1\%$ for solid Fe with respect to that expected according to pure Fe EoS (Dewaele et al., 2006). Assuming that C has a similar effect to that of S on solid Fe EoS, by using Fe-S solid alloy EoS (Sakai et al., 2012), we can infer a C content of ~ 2 at % (0.4 wt % C). In addition to the possible C solubility in solid Fe, solid Fe or Fe₃C remaining in coexistence with the liquid could affect our estimation of the C content of the liquid. However, collected diffraction patterns show only few solid peaks in

Table 1

Chemical Compositions of Fe-C Liquid Samples Measured by Rietveld Analysis of Reheated LH-DAC Samples and by Microprobe Analysis on a PEP Sample

Sample	Pressure (GPa)	Temperature (K)	wt % C	at % C
FeC_7-49	41.1 ± 1	1,380 ± 150	2.57 ± 1	10.9 ± 4
FeC_7-76	50.4 ± 1	1,600 ± 150	2.88 ± 1	12.1 ± 4
FeC_7-101	57.3 ± 1	1,630 ± 150	2.54 ± 1	10.8 ± 4
FeC5-89	40.3 ± 1	1,480 ± 150	3.01 ± 1	12.6 ± 4
FeC_15	-	-	1.52 ± 0.3	6.6 ± 1.5

Note. *P-T* conditions of reheated samples are also indicated. Example for the diffraction spectra is shown in Figure 1.

equilibrium with the liquid (Figure 1), likely accounting for less than 1 at %. The final source of the uncertainty in the estimation is related to the quality of the Rietveld analysis and potential preferred orientation (between 1 and 3 at % depending on the diffraction pattern). Overall, we estimate an error bar of ±4 at % C on the reported C content of the studied liquid (Table 1).

For samples recovered from PEP experiments, the carbon contents in quenched liquid were also determined using electron probe microanalyses (EPMA) at Centre Camparis, UPMC, Paris. We used a Cameca SX100 wavelength dispersive spectrometer (WDS) operating at 15 kV and 40 nA for a counting time of 20 s on peak and 10 s on background (Table 1). A synthesized Fe₃C sample was used as a standard for the

carbon analysis. Our recovered samples show fine dendritic textures of Fe and Fe₃C; we therefore used a defocused beam of ~20 μm to average the compositions of the quenched liquid.

2.3. Analysis of Diffuse Scattering Signal

X-ray diffuse scattering from a liquid sample could be analyzed in order to extract local structure of the liquid and has been also recently investigated to extract liquid density under high pressure (Eggert et al., 2002). More details regarding the methodology to extract density from liquid iron alloys diffuse signal under high pressures can be seen in the following articles: (Morard et al., 2013; Morard, Garbarino, et al., 2014).

Diffuse scattering patterns were acquired at ~500 K above the Fe-C eutectic melting point. The intensity of the diffuse scattering signal was observed to rise with increasing temperature above the melting point, as a direct consequence of the increased amount of liquid in the probed volume. Once the sample is fully molten, the typical exposure time required for collecting a good diffuse scattering signal is 10 s. Background signal is extracted from solid diffraction signal collected below the melting temperature (Figure 2a). Subtraction of background signal and normalization of X-ray diffraction patterns, following previously developed method (Morard, Garbarino, et al., 2014) is giving us access to the liquid structure factor $S(Q)$ (Figure 2b). Then, after a Fourier transform analysis of the $S(Q)$, the radial distribution function $g(r)$ could be obtained.

Density is extracted following the minimization of the oscillation in the short distance of the radial distribution function $g(r)$ (Eggert et al., 2002). This minimization procedure is stopped after five iterations, as convergence is reached (Figure 3). It allows to determine the liquid density while removing long-wavelength background noise present at low r region. Calculation of the position of minimal distance r_{\min} is fundamental

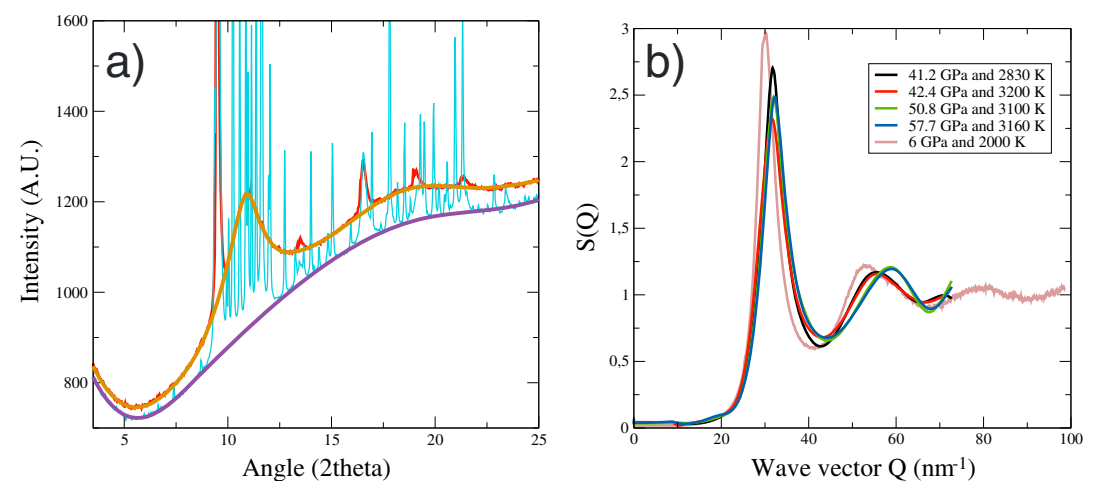


Figure 2. (a) Diffraction patterns before (turquoise) and after (red) melting in a LH-DAC experiment at 50.8 GPa. The diffuse scattering pattern from a liquid Fe-C alloy is shown by orange line, after subtracting spurious diffraction peaks from the pressure medium and solid phases. The background (purple line) was acquired from an X-ray diffraction pattern (turquoise line) before melting. (b) Structure factors $S(Q)$ of the liquids studied here at different *P-T* conditions.

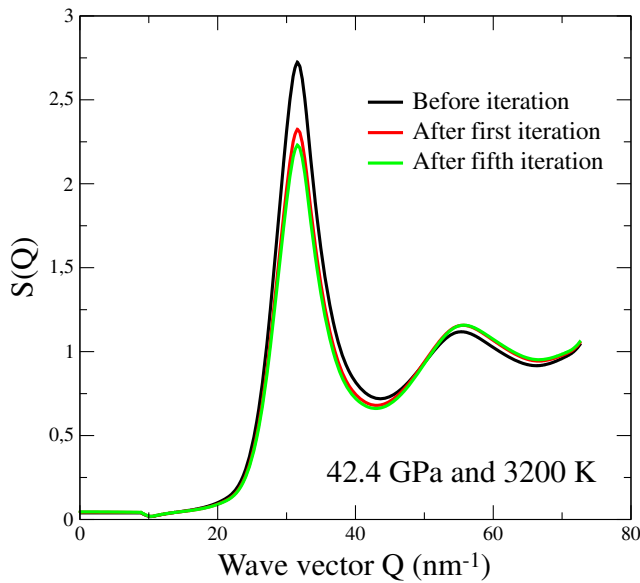


Figure 3. Structure factors $S(Q)$ at different steps of the iterative procedure. The convergence is well achieved after five steps of iterations.

3. Results and Discussion

Structure and density of liquid Fe-C alloys were measured in the PEP at 6 GPa and 2,000 K and in the LH-DAC DAC between 41 and 58 GPa at 2,800–3,200 K (Table 2). The shape of $g(r)$ is characterized by three peaks located at approximately 2.5 nm, 4.5 nm, and 6.5 nm and corresponding to the distance of the first through third coordination spheres (CS), respectively. Our results agree quite well with previous lower-pressure measurements on Fe-C liquid alloys at 6 GPa and 1,600 K (Shibazaki et al., 2015) (Figure 6a). The overall structure shows a global contraction with increasing pressure of all the coordination spheres (CS) (i.e., shifting to smaller r for the three peaks) (Figure 6a). Qualitatively, the reduction is more pronounced for the first CS than for the second and third CSs, as evident when comparing the $g(r)$ obtained at 6 GPa shifted by 0.15 nm with the $g(r)$ obtained at higher pressures (Figure 6b). These data suggest a nonuniform compression of the liquid at the local scale, with the first CS being more compressible than the rest of the structure. There could be a potential relation between solid structure corresponding to the liquid and, therefore, with the difference in compressibility observed for a , b , and c axes in solid Fe_3C (Li et al., 2002). More investigation is required in order to identify the actual compression mechanisms driving the local structure of liquid iron alloys at high pressure.

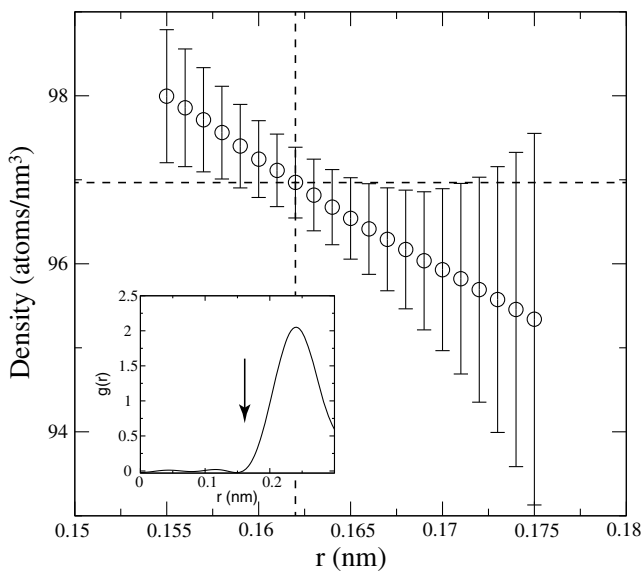


Figure 4. Calculated atomic density as a function of the minimal distance r_{\min} for Fe-C liquid alloy measured in a LH-DAC experiment. The error bar at each point is related to the figure of merit χ^2 determining the validity of the density calculation (see Morard, Garbarino, et al., (2014) for more details). The local minimum for χ^2 (minimum in the error bars) at 0.163 nm gives us the density for the studied liquid. This value of r_{\min} corresponds to the bottom of the first coordination sphere in the $g(r)$ (see inset).

to determine the density (Figure 4). This parameter represents the minimal distance for the presence of atoms, as no atom is expected to seat at distances below that of the first coordination shell of metallic liquids. More details of the data analysis procedure can be found in Morard, Garbarino, et al. (2014).

In order to compare our PEP and LH-DAC experiments, we numerically investigated the effects on the final results of different cutoff in the measured Q ranges (respectively 100 and 70 nm^{-1}). Reducing the Q range of the PEP diffuse scattering signal to that of LH-DAC experiments lowers the calculated density by less than 2 atoms/nm^3 (with respect to the initial value of 80.5 atoms/nm^3), broadens the signal, and reduces the intensity of the first coordination sphere (CS) but does not affect the position of its maximum (Figure 5).

The evaluation of the error bar on the density value is based on different parameters such as the Q range of the data, the minimal distance of the first coordination sphere, and the self-absorption from the sample (see Morard, Garbarino, et al., 2014 and Morard, Andraut, et al., 2014 for more details). In the present data set, the estimated error bar is of ± 3 atoms/nm^3 for the atomic density, corresponding to ± 250 kg/m^3 for the mass density of the present Fe-C liquids.

In our study, density measurements have been systematically performed several hundred kelvins above the liquidus temperature over a wide pressure range (from 6 to 58 GPa). This is directly reflected into a wide range of experimental temperatures (from 2,000 to 3,200 K). Other studies on density of liquid Fe-C alloys (Shimoyama et al., 2013; Terasaki et al., 2010) have been performed using large-volume presses at significantly lower temperatures compared to the present LH-DAC data set. The easiest way to directly compare data sets spanning a wide P - T range is to reduce them along an isotherm. This can be done by using the coefficient of thermal expansion of pure molten Fe that was established recently (Assael et al., 2006) and that has already been used for extrapolations to 3,000 K (Shimoyama et al., 2013; Terasaki et al.,

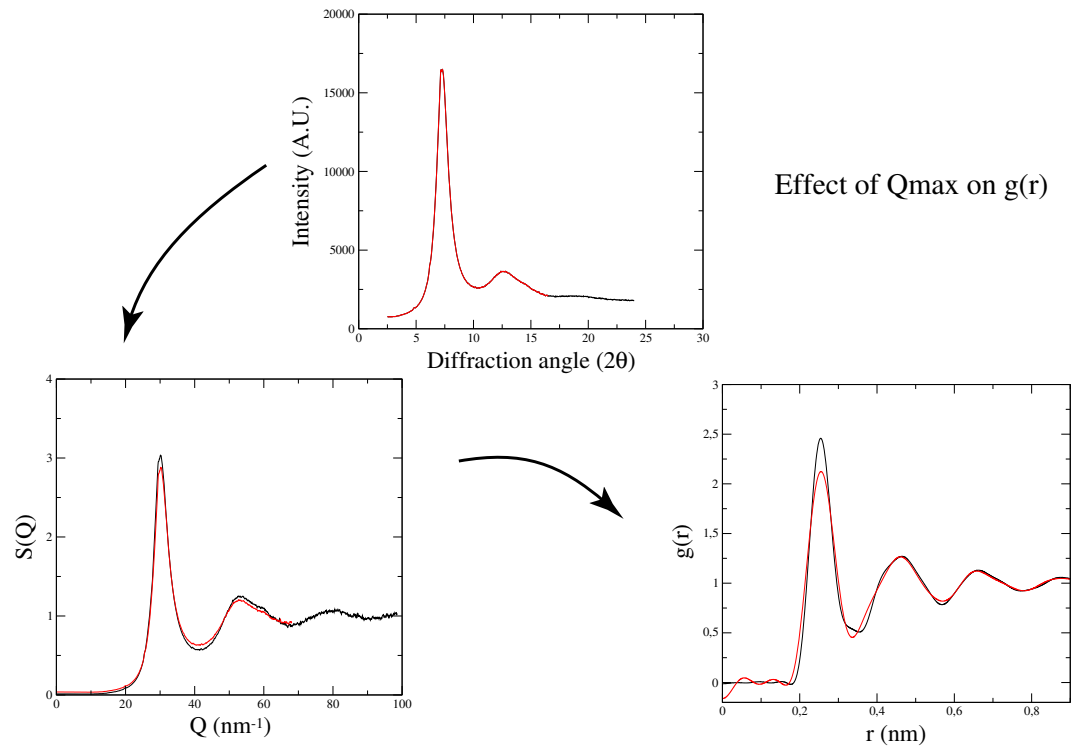


Figure 5. Effects on the obtained $g(r)$ from the modification of the Q ranges to 100 nm^{-1} in black and to 70 nm^{-1} in red. The peak positions are not affected, but their respective height and width are modified.

2010). We preferred using the value of pure molten Fe ($d\rho/dT = 9.26 \text{ kg m}^{-3} \text{ K}^{-1}$) rather than the measurements made on liquid Fe-C alloys ($d\rho/dT = 5.66 \text{ kg m}^{-3} \text{ K}^{-1}$) (Jimbo & Cramb, 1993), because (i) such a Fe-C data set spans over a limited temperature range (300 K instead of 700 K) and (ii) large discrepancies exist between the literature studies regarding the thermal expansion of liquid Fe-C alloys, even at ambient pressure (Jimbo & Cramb, 1993, and references therein).

We assumed that αK_T was constant for the Fe-C alloy over the studied pressure range, where α is the thermal expansion coefficient and K_T is the isothermal bulk modulus at a temperature T . This classical assumption is verified for liquid iron, for which $\alpha K_T(1 \text{ bar}) = 1.08 \times 10^{-2}$ ($K_T = 82 \text{ GPa}$ at $1,900 \text{ K}$ (Hixson et al., 1990), when $\alpha = 1.32 \times 10^{-4}$ (Assael et al., 2006)) and $\alpha K_T = 0.95 \times 10^{-2}$ at 150 GPa and $4,000 \text{ K}$ (Ichikawa et al., 2014). We assume that our Fe-C alloys have a similar αK_T value of $\sim 10^{-2}$. Using this value, we can collapse our density measurements, performed at different temperatures to a common $3,000 \text{ K}$ isotherm (Table 2). Our experimental density measurements performed in the PEP then fall into relative agreement with previously published results (Shimoyama et al., 2013; Terasaki et al., 2010) (Figure 7). This also allows our data set to be

Table 2
Pressure and Temperature Conditions for the Density Measurements

	Pressure (GPa)	Temperature (K)	Carbon content (at %)	Density (kg/m ³)	Density corrected at 3,000 K (kg/m ³)
FeC_7-49	42.4 ± 1	$3,200 \pm 150$	10.9 ± 4	$7,880 \pm 250$	$7,950 \pm 250$
FeC_7-76	50.8 ± 1	$3,100 \pm 150$	12.1 ± 4	$8,140 \pm 250$	$8,170 \pm 250$
FeC_7-101	57.7 ± 1	$3,160 \pm 150$	10.8 ± 4	$8,320 \pm 250$	$8,370 \pm 250$
FeC5-89	41.2 ± 1	$2,830 \pm 150$	12.6 ± 4	$7,860 \pm 250$	$7,800 \pm 250$
FeC_15	6 ± 0.5	$2,000 \pm 100$	6.6 ± 1.5	$7,220 \pm 250$	$6,480 \pm 250$

Note. Density has been extracted from the diffuse scattering of the liquid following previously established method (Morard, Garbarino, et al., 2014).

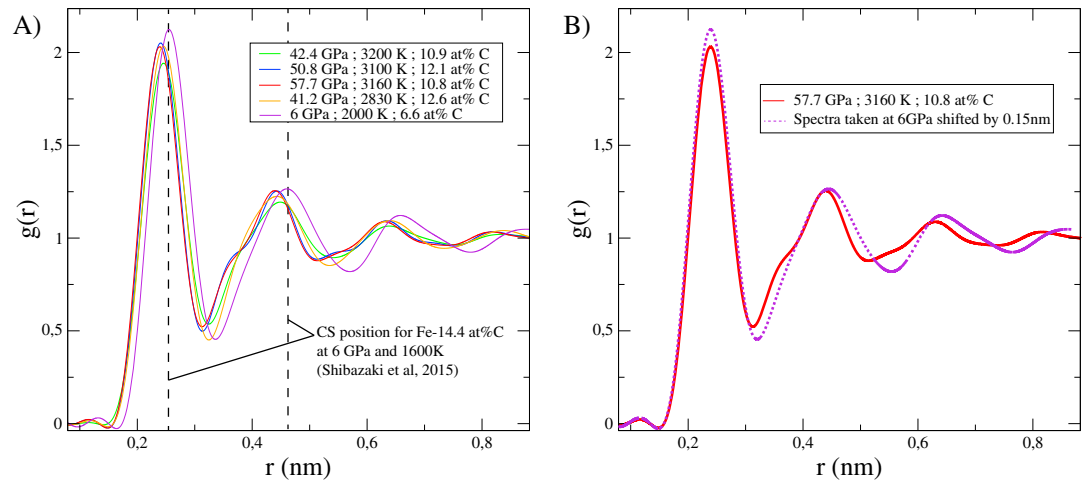


Figure 6. (a) Liquid structure of Fe-C alloys as a function of pressure. The PEP experiment at 6 GPa has been calculated using the same Q range (up to 7 \AA^{-1}) as is available from the LH-DAC experiments. The position of the first two CSs at 6 GPa from a previous publication (Shibazaki et al., 2015) is indicated by the dashed vertical lines, which are in good agreement with our results. To better highlight the compression mechanism, we also show the $g(r)$ obtained at 6 GPa shifted by 0.15 nm (dashed curve), so as to have the position of the first maximum overlapping those of higher pressure results. (b) Comparison between low-pressure (6 GPa) liquid structure, shifted by 0.15 nm, and higher-pressure liquid structure. This evidences a differential compression behavior between the different coordination spheres.

fitted to an isothermal compression curve, using a third-order Birch-Murnaghan EoS (Figure 7). The fit is anchored to an ambient pressure density at 3,000 K of $\rho_{0,3000\text{K}} = 6,000 \text{ kg/m}^3$, based on a combination of metallurgical data sets (Assael et al., 2006; Jimbo & Cramb, 1993). We fitted our data set using two different values for the pressure derivative of the bulk modulus (K'), $K' = 4$ and $K' = 6$, leading to different values of the bulk modulus at 1 bar ($K_T = 3000\text{K}, 0 = 89 \text{ GPa}$ for $K' = 4$ and $K_T = 3000\text{K}, 0 = 65 \text{ GPa}$ for $K' = 6$).

At ambient pressure, carbon does not seem to significantly affect the density of liquid Fe: the change of liquid Fe density with either 6 at % C or 12 at % C has been reported to be less than 100 kg/m^3 (Jimbo & Cramb,

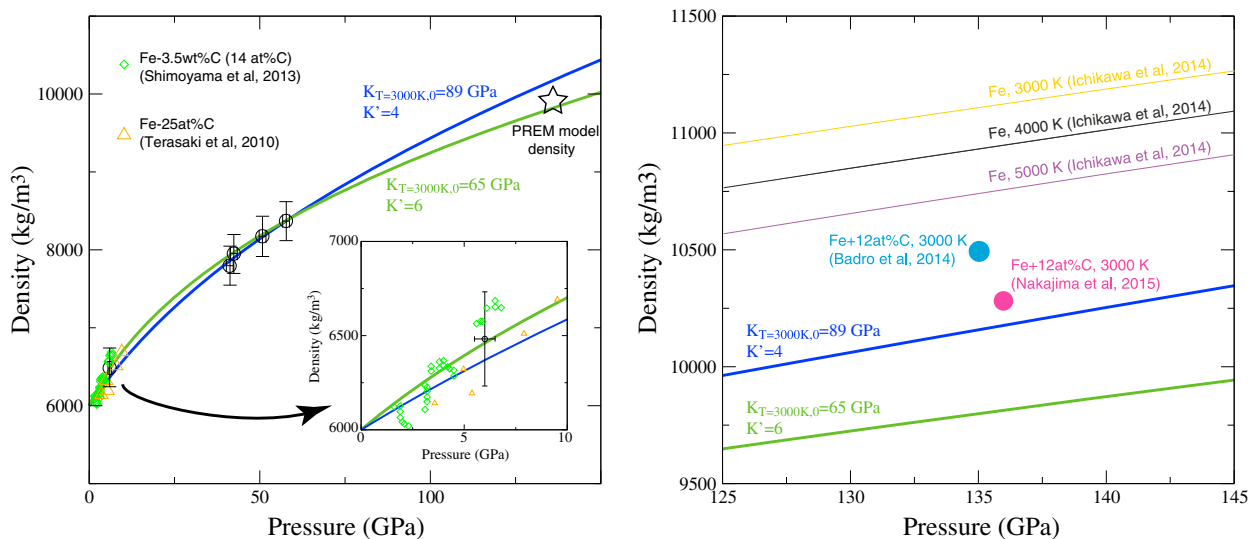


Figure 7. (left) Density of liquid Fe-C alloys as a function of pressure determined here (Table 1), corrected to 3,000 K (see text for details). Two EoS models with different K' and K_{T0} have been used to extrapolate the density of the Fe-C alloy to the CMB pressure. For comparison, the low-pressure densities (Shimoyama et al., 2013; Terasaki et al., 2010) have been corrected to fall on the same 3,000 K isotherm using the coefficient of thermal expansion for pure liquid Fe (Assael et al., 2006). The density of the Earth's core at the CMB from the PREM model is indicated as a star symbol. (inset) Zoom over the lower-pressure range. (right) Expanded view around the CMB pressure showing our extrapolated EoS and the comparison with previous studies (Badro et al., 2014; Ichikawa et al., 2014; Nakajima et al., 2015).

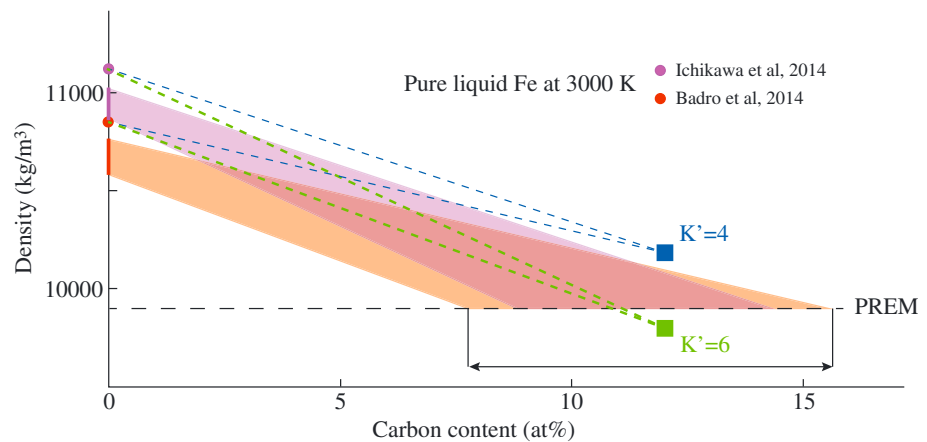


Figure 8. Density reduction as a function of carbon content at the CMB pressure of 136 GPa. Two different references for pure iron are taken from Badro et al. (2014) and Ichikawa et al. (2014). The density reduction is calculated at 3,000 K based on the two EoSs shown in Figure 3 ($K' = 4$ and $K' = 6$). The two shaded areas represent the density reduction domains in a temperature range between 3,500 K and 4,500 K based on the two references for pure Fe liquid density at the CMB pressure. The intersection between these domains and the density of PREM at the CMB (indicated by the horizontal dashed line) indicates a composition range between 8 and 16 at % C (1.8–3.7 wt % C) expected to explain outer core densities under the hypothesis of C being the only light element in the Earth's outer core.

1993), which is small relative to the uncertainties. Such behavior seems valid up to 3 GPa (Shimoyama et al., 2016). The present results are in reasonable agreement with previous density measurements on liquid Fe-C alloys with 14 at % C (3.5 wt %) (Shimoyama et al., 2013) and 25 at % C (Fe_3C) (Terasaki et al., 2010) as measured by X-ray absorption imaging (Figure 7, left). Structural changes observed in liquid Fe-C alloys (Shibazaki et al., 2015) may imply some discontinuity in density evolution as observed by Shimoyama et al. (2013). A closer look to the low-pressure range (Figure 7, left, inset) shows that our density data point do not support such strong density shift, although this cannot be excluded within our error bars.

Extrapolation to higher pressures of our density measurements are quite close to density calculated from sound velocity measurements on liquid Fe-C alloys in LH-DAC (Nakajima et al., 2015) and fall somewhat below the values obtained by molecular dynamics simulations (Badro et al., 2014) (Figure 7, right). However, in view of the relatively large extrapolation from our highest pressure point (58 GPa) to the core-mantle boundary (CMB) pressure (136 GPa), we can consider these two data sets in overall agreement with our experimental results. However, it should be noted that our previous density measurements on Fe-S and Fe-Si alloys (Morard et al., 2013) were also systematically lower than ab initio calculations (Badro et al., 2014).

The density measurements presented here can be used to discuss the carbon content of the Earth's core. In particular, we can propose an upper bound under the hypothesis in which carbon is the sole light element in the outer core. The density of pure Fe at the CMB is taken from recent ab initio calculations (Badro et al., 2014; Ichikawa et al., 2014). Here we assume a linear dependence of density on C content in the 0–15 at %, as suggested by ab initio calculations (Badro et al., 2014). However, it should be noticed that this approximation may not be strictly correct on thermodynamic basis and therefore cannot be extrapolated over a large compositional range. Assuming this linear relation for density as a function of C content between our measurements (~12 at % C) and calculations on pure Fe, we found a density reduction at 136 GPa and 3,000 K between ~60 and ~110 $\text{kg/m}^3/\text{at} \% \text{C}$ (Figure 8). This effect is larger than that observed at ambient pressure (17 $\text{kg/m}^3/\text{at} \% \text{C}$) (Jimbo & Cramb, 1993). The augmented density reduction suggests that carbon inclusion increases the bulk modulus of liquid iron, supporting similar observations by sound velocity measurements for liquid Fe-C alloys (Nakajima et al., 2015).

Next, we assume a CMB temperature in the range of 3,500–4,500 K that accounts for the absence of extended mantle melting at the CMB (Andrault et al., 2014; Fiquet et al., 2010; Pradhan et al., 2015). In this case, the carbon content required to explain the density deficit is between 16 at % C (3.6 wt % C) and 8 at % C (1.8 wt % C) (Figure 8). However, this solution seems not acceptable. Indeed, according to sound velocity

measurements on liquid Fe-C alloys (Nakajima et al., 2015), an alloy with such a high carbon content would have a velocity much higher than seismological observations; that is, carbon increases sound velocity and PREM values are expected to be attained for an alloy with ~5 at % C (0.9 wt % C) (Nakajima et al., 2015). Our conclusions thus support those of recent calculations on solid Fe-C alloys (Caracas, 2015) on the point that carbon cannot be considered the only light element in the core.

4. Conclusions

Structure and density of liquid Fe-C alloys have been measured up to 58 GPa and 3,200 K by in situ X-ray diffraction. Pressure-induced structural changes evidence a nonuniform compression for the first three coordination shells, with a higher compression rate for the first than for the second or the third. Density of liquid Fe-C alloys (~12 at % C) has been determined up to the highest pressure so far, increasing the pressure range of experimental measurements by 1 order of magnitude. Obtained data are in relatively good agreement with previously published low-pressure results and can be fit with a third-order Birch-Murnaghan equation of state. The Extrapolation with the EoS to CMB pressure and temperature conditions suggests that 8–16 at % C (1.8–3.7 wt % C) would be necessary to explain the outer core density if carbon is the only light element in the core. However, a liquid alloy with such a high carbon content is expected to have a velocity much higher than that of the outer core (Nakajima et al., 2015).

We also notice that classic estimations of carbon content in the Earth's core based on geochemical and cosmochemical arguments limit carbon to ~0.2 wt % (McDonough, 2003) up to ~1 wt % (Wood et al., 2013). A hypothetical model with an Earth's outer core containing 1.8–3.7 wt % C and an associated inner core made of Fe₇C₃ (Prescher et al., 2015) would call for a drastic revision of the estimated carbon budget of the Earth and is incompatible with the current understanding of Earth's accretion and differentiation processes. We can then conclude that it is unlikely that carbon is the only light element in the core and that the presence of other light elements (e.g., O, Si, H, and S) is required.

Acknowledgments

The authors thank Stany Bauchau (ESRF) for his help with the X-ray experiments; Patrick Ochinn and Loic Perrière (Institut de Chimie et des Matériaux de Paris-Est, Paris, France) for the synthesis of starting materials. This work was supported by the Planetlab program of the French National Research Agency (ANR), grant ANR-12-BS04-001504 and the European Research Council (ERC) under the European Union's Horizon 2020 research and innovation programme (grant agreement 637748). This work was also supported through a fellowship awarded to O. T. L. at Bristol from the UK Natural Environment Research Council (NE/J018945/1). Data used in this study are available upon request to Guillaume Morard (guillaume.morard@impmc.upmc.fr).

References

- Andraut, D., Pesce, G., Bouhifd, M. A., Bolfan-Casanova, N., Hénot, J.-M., & Mezouar, M. (2014). Melting of subducted basalt at the core-mantle boundary. *Science*, *344*(6186), 892–895. <https://doi.org/10.1126/science.1250466>
- Assael, M. J., Kakosimos, K., Banish, R. M., Brillo, J., Egry, I., Brooks, R., ... Wakeham, W. A. (2006). Reference data for the density and viscosity of liquid aluminum and liquid iron. *Journal of Physical and Chemical Reference Data*, *35*(1), 285–300. <https://doi.org/10.1063/1.2149380>
- Badro, J., Cote, A. S., & Brodholt, J. P. (2014). A seismologically consistent compositional model of Earth's core. *Proceedings of the National Academy of Sciences*, *111*(21), 7542–7545. <https://doi.org/10.1073/pnas.1316708111>
- Boehler, R., & De Hantsetters, K. (2004). New anvil designs in diamond-cells. *High Pressure Research*, *24*(3), 391–396. <https://doi.org/10.1080/08957950412331323924>
- Besson, J.-M., Hamel, G., Grima, P., Nelmel, R. J., Loveday, J. S., Hull, S., & Hausermann, D. (1992). A Large Volume Pressure Cell for High Temperatures. *High Pressure Research*, *8*, 625.
- Campbell, A. J., Danielson, L., Richter, K., Seagle, C. T., Wang, Y., & Prakapenka, V. B. (2009). High pressure effects on the iron-iron oxide and nickel-nickel oxide oxygen fugacity buffers. *Earth and Planetary Science Letters*, *286*(3-4), 556–564. <https://doi.org/10.1016/j.epsl.2009.07.022>
- Caracas, R. (2015). The influence of hydrogen on the seismic properties of solid iron. *Geophysical Research Letters*, *42*(10), 3780–3785. <https://doi.org/10.1002/2015GL063478>
- Chen, B., Li, Z., Zhang, D., Liu, J., Hu, M. Y., Zhao, J., ... Li, J. (2014). Hidden carbon in Earth's inner core revealed by shear softening in dense Fe₇C₃. *Proceedings of the National Academy of Sciences*, *111*(50), 17,755–17,758. <https://doi.org/10.1073/pnas.1411154111>
- Chi, H., Dasgupta, R., Duncan, M. S., & Shimizu, N. (2014). Partitioning of carbon between Fe-rich alloy melt and silicate melt in a magma ocean—Implications for the abundance and origin of volatiles in earth, Mars, and the moon. *Geochimica et Cosmochimica Acta*, *139*, 447–471. <https://doi.org/10.1016/j.gca.2014.04.046>
- Dasgupta, R., & Walker, D. (2008). Carbon solubility in core melts in a shallow magma ocean environment and distribution of carbon between the Earth's core and the mantle. *Geochimica et Cosmochimica Acta*, *72*(18), 4627–4641. <https://doi.org/10.1016/j.gca.2008.06.023>
- De Koker, N., Steinle-Neumann, G., & Vlcek, V. (2012). Electrical resistivity and thermal conductivity of liquid Fe alloys at high P and T, and heat flux in Earth's core. *Proceedings of the National Academy of Sciences of the United States of America*, *109*(11), 4070–4073. <https://doi.org/10.1073/pnas.1111841109>
- Dewaele, A., Belonoshko, A. B., Garbarino, G., Occelli, F., Bouvier, P., Hanfland, M., & Mezouar, M. (2012). High-pressure-high-temperature equation of state of KCl and KBr. *Physical Review B: Condensed Matter and Materials Physics*, *85*(21), 1–7. <https://doi.org/10.1103/PhysRevB.85.214105>
- Dewaele, A., Loubeyre, P., Occelli, F., Mezouar, M., Dorogokupets, P. I., & Torrent, M. (2006). Quasihydrostatic equation of state of iron above 2 Mbar. *Physical Review Letters*, *97*(21), 29–32. <https://doi.org/10.1103/PhysRevLett.97.215504>
- Eggert, J., Weck, G., Loubeyre, P., & Mezouar, M. (2002). Quantitative structure factor and density measurements of high-pressure fluids in diamond anvil cells by X-ray diffraction: Argon and water. *Physical Review B*, *65*(17), 1–12. <https://doi.org/10.1103/PhysRevB.65.174105>
- Fei, Y., & Brosh, E. (2014). Experimental study and thermodynamic calculations of phase relations in the Fe-C system at high pressure. *Earth and Planetary Science Letters*, *408*, 155–162. <https://doi.org/10.1016/j.epsl.2014.09.044>

- Fiquet, G., Auzende, A. L., Siebert, J., Corgne, A., Bureau, H., Ozawa, H., & Garbarino, G. (2010). Melting of peridotite to 140 gigapascals. *Science*, 329(5998), 1516–1518. <https://doi.org/10.1126/science.1192448>
- Fischer, R. A., Nakajima, Y., Campbell, A. J., Frost, D. J., Harries, D., Langenhorst, F., ... Rubie, D. C. (2015). High pressure metal-silicate partitioning of Ni, Co, V, Cr, Si, and O. *Geochimica et Cosmochimica Acta*, 167, 177–194. <https://doi.org/10.1016/j.gca.2015.06.026>
- Hammersley, A. P., Svensson, S. O., Hanfland, M., Fitch, A. N., & Hausermann, D. (1996). Two-dimensional detector software: From real detector to idealised image or two-theta scan. *High Pressure Research*, 14(4-6), 235–248. <https://doi.org/10.1080/08957959608201408>
- Hixson, R. S., Winkler, M. A., & Hodgdon, M. L. (1990). Sound speed and thermophysical properties of liquid iron and nickel. *Physical Review B*, 42(10), 6485–6491. <https://doi.org/10.1103/PhysRevB.42.6485>
- Ichikawa, H., Tschuchiya, T., & Tange, Y. (2014). The P-V-T equation of state and thermodynamic properties of liquid iron. *Journal of Geophysical Research: Solid Earth*, 119(1), 240–252. <https://doi.org/10.1002/2013JB010732>
- Jimbo, I., & Cramb, A. W. (1993). The density of liquid iron-carbon alloys. *Metallurgical Transactions B*, 24(1), 5–10. <https://doi.org/10.1007/BF02657866>
- Klotz, S., Strässle, Th., Rousse, G., Hamel, G., & Pomjakushin, V. (2005). Angle-Dispersive Neutron Diffraction under High Pressure to 10 GPa. *Applied Physics Letters*, 86(3), 1–3. <https://doi.org/10.1063/1.1855419>
- Li, J., Mao, H. K., Fei, Y., Gregoryanz, E., Eremets, M., & Zha, C. S. (2002). Compression of Fe₃C to 30 GPa at room temperature. *Physics and Chemistry of Minerals*, 29(3), 166–169. <https://doi.org/10.1007/s00269-001-0224-4>
- Liu, J., Li, L., Hrubciak, R., & Smith, J. S. (2016). Origins of ultralow velocity zones through slab-derived metallic melt. *Proceedings of the National Academy of Sciences*, 113(20), 5547–5551. <https://doi.org/10.1073/pnas.1519540113>
- Liu, J., Lin, J.-F., Prakashenka, V., Prescher, C., & Yoshino, T. (2016). Phase relations of Fe₃C and Fe₇C₃ up to 185 GPa and 5200 K: Implication for the stability of iron carbide in the Earth's core. *Geophysical Research Letters*, 43(24), 12,415–12,422. <https://doi.org/10.1002/2016GL071353>
- Lord, O. T., Walter, M. J., Dasgupta, R., Walker, D., & Clark, S. M. (2009). Melting in the Fe-C system to 70 GPa. *Earth and Planetary Science Letters*, 284(1-2), 157–167. <https://doi.org/10.1016/j.epsl.2009.04.017>
- McDonough, W. F. (2003). Compositional model for the Earth's Core. *Treatise on Geochemistry*, 2, 547–568. <https://doi.org/10.1016/B0-08-043751-6/02015-6>
- Mezouar, M., Crichton, W. A., Bauchau, S., Thurel, F., Witsch, H., Torrecillas, F., ... Borel, C. (2005). Development of a new state-of-the-art beamline optimized for monochromatic single crystal and powder X-ray diffraction under extreme conditions at the ESRF. *Journal of Synchrotron Radiation*, 12(5), 659–664. <https://doi.org/10.1107/S0909049505023216>
- Mezouar, M., Faure, P., Crichton, W., Rambert, N., Sitaud, B., Bauchau, S., & Blattmann, G. (2002). Multichannel collimator for structural investigation of liquids and amorphous materials at high pressures and temperatures. *The Review of Scientific Instruments*, 73(10), 3570–3574. <https://doi.org/10.1063/1.1505104>
- Mezouar, M., Le Bihan, T., Libotte, H., Le Godec, Y., & Häusermann, D. (1999). Paris-Edinburgh large-volume cell coupled with a fast imaging plate system for structural investigation at high pressure and high temperature. *Journal of Synchrotron Radiation*, 6(6), 1115–1119. <https://doi.org/10.1107/S0909049599010651>
- Mookherjee, M. (2011). Elasticity and anisotropy of Fe₃C at high pressures. *American Mineralogist*, 96(10), 1530–1536. <https://doi.org/10.2138/am.2011.3917>
- Morard, G., Andrault, D., Antonangeli, D., & Bouchet, J. (2014). Properties of iron alloys under the Earth's core conditions. *Comptes Rendus Geoscience*, 346(5-6), 130–139. <https://doi.org/10.1016/j.crte.2014.04.007>
- Morard, G., Andrault, D., Antonangeli, D., Nakajima, Y., Auzende, A. L., Boulard, E., ... Mezouar, M. (2017). Fe–FeO and Fe–Fe₃C melting relations at Earth's core–mantle boundary conditions: Implications for a volatile-rich or oxygen-rich core. *Earth and Planetary Science Letters*, 473, 94–103. <https://doi.org/10.1016/j.epsl.2017.05.024>
- Morard, G., Andrault, D., Guignot, N., Siebert, J., Garbarino, G., & Antonangeli, D. (2011). Melting of Fe–Ni–Si and Fe–Ni–S alloys at megabar pressures: Implications for the core–mantle boundary temperature. *Physics and Chemistry of Minerals*, 38(10), 767–776. <https://doi.org/10.1007/s00269-011-0449-9>
- Morard, G., Garbarino, G., Antonangeli, D., Andrault, D., Guignot, N., ... Petitgirard, S. (2014). Density measurements and structural properties of liquid and amorphous metals under high pressure. *High Pressure Research*, 34(1), 9–21. <https://doi.org/10.1080/08957959.2013.860137>
- Morard, G., Mezouar, M., Bauchau, S., Álvarez-Murga, M., Hodeau, J. L., & Garbarino, G. (2011). High efficiency multichannel collimator for structural studies of liquids and low-Z materials at high pressures and temperatures. *The Review of Scientific Instruments*, 82(2), 023904. <https://doi.org/10.1063/1.3551988>
- Morard, G., Mezouar, M., Rey, N., Poloni, R., Merlen, A., Le Floch, S., ... Fiquet, G. (2007). Optimization of Paris-Edinburgh press cell assemblies for in situ monochromatic X-ray diffraction and X-ray absorption. *High Pressure Research*, 27(2), 223–233. <https://doi.org/10.1080/08957950601183553>
- Morard, G., Sanloup, C., Fiquet, G., Mezouar, M., Rey, N., Poloni, R., & Beck, P. (2007). Structure of eutectic Fe–FeS melts to pressures up to 17 GPa: Implications for planetary cores. *Earth and Planetary Science Letters*, 263(1-2), 128–139. <https://doi.org/10.1016/j.epsl.2007.09.009>
- Morard, G., Siebert, J., Andrault, D., Guignot, N., Garbarino, G., Guyot, F., & Antonangeli, D. (2013). The Earth's core composition from high pressure density measurements of liquid iron alloys. *Earth and Planetary Science Letters*, 373, 169–178. <https://doi.org/10.1016/j.epsl.2013.04.040>
- Nakajima, Y., Imada, S., Hirose, K., Komabayashi, T., Ozawa, H., Tateno, S., ... Baron, A. Q. R. (2015). Carbon-depleted outer core revealed by sound velocity measurements of liquid iron–carbon alloy. *Nature Communications*, 6(8942). <https://doi.org/10.1038/ncomms9942>
- Nakajima, Y., Takahashi, E., Sata, N., Nishihara, Y., Hirose, K., Funakoshi, K. I., & Ohishi, Y. (2011). Thermoelastic property and high-pressure stability of Fe₇C₃: Implication for iron-carbide in the Earth's core. *American Mineralogist*, 96(7), 1158–1165. <https://doi.org/10.2138/am.2011.3703>
- Nakajima, Y., Takahashi, E., Suzuki, T., & Funakoshi, K. (2009). "Carbon in the core" revisited. *Physics of the Earth and Planetary Interiors*, 174(1-4), 202–211. <https://doi.org/10.1016/j.pepi.2008.05.014>
- Poirier, J. P. (1994). Light elements in the Earth's outer core: A critical review. *Physics of the Earth and Planetary Interiors*, 85(3-4), 319–337. [https://doi.org/10.1016/0031-9201\(94\)90120-1](https://doi.org/10.1016/0031-9201(94)90120-1)
- Pradhan, G. K., Fiquet, G., Siebert, J., Auzende, A.-L., Morard, G., Antonangeli, D., & Garbarino, G. (2015). Melting of MORB at core–mantle boundary. *Earth and Planetary Science Letters*, 431, 247–255. <https://doi.org/10.1016/j.epsl.2015.09.034>
- Prescher, C., Dubrovinsky, L., Bykova, E., Kuppenko, I., Glazyrin, K., Kantor, A., ... Hanfland, M. (2015). High Poisson's ratio of Earth's inner core explained by carbon alloying. *Nature Geoscience*, 8(3), 220–223. <https://doi.org/10.1038/ngeo2370>

- Sakai, T., Ohtani, E., Kamada, S., Terasaki, H., & Hirao, N. (2012). Compression of $\text{Fe}_{88.1}\text{Ni}_{9.1}\text{S}_{2.8}$ alloy up to the pressure of Earth's inner core. *Journal of Geophysical Research*, 117(B2), B02210. <https://doi.org/10.1029/2011JB008745>
- Schultz, E., Mezouar, M., Crichton, W., Bauchau, S., Blattmann, G., Andrault, D., ... Loubeyre, P. (2005). Double-sided laser heating system for in situ high pressure–high temperature monochromatic X-ray diffraction at the ESRF. *High Pressure Research*, 25(1), 71–83. <https://doi.org/10.1080/08957950500076031>
- Shibazaki, Y., Kono, Y., & Fei, Y. (2015). Microscopic structural change in a liquid Fe–C alloy of ~5 GPa. *Geophysical Research Letters*, 42(13), 5236–5242. <https://doi.org/10.1002/2015GL064271>
- Shimoyama, Y., Terasaki, H., Ohtani, E., Urakawa, S., Takubo, Y., Nishida, K., ... Katayama, Y. (2013). Density of Fe–3.5wt% C liquid at high pressure and temperature and the effect of carbon on the density of the molten iron. *Physics of the Earth and Planetary Interiors*, 224, 77–82. <https://doi.org/10.1016/j.pepi.2013.08.003>
- Shimoyama, Y., Terasaki, H., Urakawa, S., Takubo, Y., Kuwabara, S., Kishimoto, S., ... Kondo, T. (2016). Thermoelastic properties of liquid Fe–C revealed by sound velocity and density measurements at high pressure. *Journal of Geophysical Research: Solid Earth*, 121(11), 7984–7995. <https://doi.org/10.1002/2016JB012968>
- Siebert, J., Badro, J., Antonangeli, D., & Ryerson, F. J. (2013). Terrestrial accretion under oxidizing conditions. *Science*, 339(6124), 1194–1197. <https://doi.org/10.1126/science.1227923>
- Terasaki, H., Nishida, K., Shibazaki, Y., Sakamaki, T., Suzuki, A., Ohtani, E., & Kikegawa, T. (2010). Density measurement of Fe_3C liquid using X-ray absorption image up to 10 GPa and effect of light elements on compressibility of liquid iron. *Journal of Geophysical Research*, 115(B6), B06207. <https://doi.org/10.1029/2009JB006905>
- Utsumi, W., Weidner, D. J., & Liebermann, R. C. (1998). Volume measurement of MgO at high pressures and high temperatures. *Geophysical Monograph*, 101, 327–333. <https://doi.org/10.1029/GM101p0327>
- Wood, B. J., Li, J., & Shahar, A. (2013). Carbon in the Core: Its influence on the properties of core and mantle. *Reviews in Mineralogy and Geochemistry*, 75(1), 231–250. <https://doi.org/10.2138/rmg.2013.75.8>